Article

A Building Information Modeling Approach to Integrate Geomatic Data for the Documentation and Preservation of Cultural Heritage

Mercedes Solla [1,2,*], **Luisa M. S. Gonçalves** [3,4], **Gil Gonçalves** [4,5], **Carina Francisco** [4], **Iván Puente** [2], **Paulo Providência** [4,6], **Florindo Gaspar** [7] **and Hugo Rodrigues** [8]

1   CINTECX, GeoTECH Group, Universidade de Vigo, 36310 Vigo, Spain
2   Defense University Center, Spanish Naval Academy, 36900 Marín, Spain; ipuente@cud.uvigo.es
3   ESTG, Polytechnic Institute of Leiria, Nova IMS University, 2411-901 Leiria, Portugal;
    luisa.goncalves@ipleiria.pt
4   INESC-Coimbra, Department of Electrical and Computer Engineering, 3030-290 Coimbra, Portugal;
    gil@mat.uc.pt (G.G.); carina@mat.uc.pt (C.F.); provid@dec.uc.pt (P.P.)
5   Department of Mathematics, University of Coimbra, 3001-501 Coimbra, Portugal
6   Department of Civil Engineering, University of Coimbra, 3030-788 Coimbra, Portugal
7   CDRSP, ESTG, Polytechnic of Leiria, 2411-901 Leiria, Portugal; florindo.gaspar@ipleiria.pt
8   RISCO, Civil Engineering Department, University of Aveiro, 3810-193 Aveiro, Portugal; hrodrigues@ua.pt
*   Correspondence: merchisolla@uvigo.es

check for
updates

Abstract: Non-destructive testing (NDT) techniques play an important role in the characterization and diagnosis of historic buildings, keeping in mind their conservation and possible rehabilitation. This paper presents a new approach that merges building information modeling (BIM) with environment geospatial data obtained by several non-destructive techniques, namely terrestrial laser scanning, ground-penetrating radar, infrared thermography, and the automatic classification of pathologies based on RGB (red, green, blue) imaging acquired with an unmanned aircraft system (UAS). This approach was applied to the inspection of the Monastery of Batalha in Leiria, Portugal, a UNESCO World Heritage Site. To assess the capabilities of each technique, different parts of the monastery were examined, namely (i) part of its west façade, including a few protruding buttresses, and (ii) the masonry vaults of the Church (nave, right-hand aisle, and transept) and the Founder's Chapel. After describing the employed techniques, a discussion of the optimization, treatment and integration of the acquired data through the BIM approach is presented. This work intends to contribute to the application of BIM in the field of cultural heritage, aiming at its future use in different activities such as facility management, support in the restoration and rehabilitation process, and research.

Keywords: nondestructive evaluation; material characterization; cultural heritage; aerial surveying; image classification; laser scanning; IRT; GPR; integration; BIM

1. Introduction

Built cultural heritage is delicate and, once lost, it is unrecoverable. It consists of architectural structures and other constructions that constitute the basic record of past human activities and, as such, should be protected [1]. The conservation and rehabilitation of historical buildings must be particularly cautious with the preservation of their singular characteristics. Hence, each such building must be fully examined in order to identify those unique characteristics: structure type, construction methods

and enlargement, reconstruction and restoration interventions over time, materials employed and their source, types of use, etc.

One of the key tasks in such survey is the detection and identification of stone anomalies. Several researchers have studied the anomalies of stone in buildings, e.g., black crusts [2], patina [3], biological colonization [4], soiling [5], alveolization [6], scaling [7] and delamination [8]. The inspection and monitoring of these anomalies are crucial to plan maintenance and repairs, or even to investigate air pollution [2], and should desirably employ suitable techniques to provide, as much as possible, fast and accurate results.

Conservation and restoration interventions should be performed by multidisciplinary research teams due to (i) the diversity of involved information and knowledge, and (ii) the different perspective that archaeologists, historians and art historians, engineers, architects, etc., are expected to have about a specific intervention. To record the captured heterogeneous datasets such as multispectral images, geophysical data or 3D laser scanning data, a hybrid approach consisting of different media, e.g., one for each type of data, is often employed. This renders the extraction of information from the different media a rather complex task, even when they refer to the same zone or element of the building or structure. As a most convenient and efficient alternative, an integrated approach collecting in a unique medium the whole information about a built heritage construction should be used to support data and documentation and to assist in its preservation. However, several persistent challenges must be faced: (i) the combination of entirely different types of data, (ii) the huge amount of data that most of the above technologies produce, and (iii) 3D digital documentation of built heritage.

The use of a building information modeling (BIM) process can greatly contribute to the management and planning of the conservation and restoration works of historic buildings [9–11], because it allows for the geospatial integration of datasets obtained by different techniques and involving distinct areas of knowledge, such as architecture, archaeology, engineering, materials and remote detection [12,13]. There have been several application studies in this field, such as the Corral del Carbón in Granada, Spain [14], the Panagia Chryseleousa Church in Foinikaria, Cyprus [15], and the Basilica di Collemaggio in Aquila, Italy, struck by a severe earthquake in 2009 [16]. The main objective in these cases, and this is a general trend, was to prepare tools to support the development of a dedicated rehabilitation project or the planning and scheduling of conservation and restoration works.

Non-destructive testing (NDT) techniques play an important role in the characterization of historic buildings and detection of pathologies, aiming at their conservation and possible rehabilitation. Most commonly, the external assessment of the construction can be carried out using NDT methods such as photogrammetry, multispectral, hyperspectral and/or infrared thermographic (IRT) imaging, based upon unmanned aircraft system (UAS) surveys or terrestrial laser scanning (TLS) technologies. These techniques allow the building geometry to be ascertained and pathologies to be identified such as moisture, material degradation, cracking and deflections or tilting of vertical members [17–24]. The internal (i.e., through-the-thickness) assessment of the elements of the structure is more complex, but it can be accomplished by geophysical techniques. Among these, ground-penetrating radar (GPR) is a fast data acquisition technique that has been commonly employed for high-resolution imaging in many archaeological and cultural heritage applications [25]. In this framework, GPR has proved its aptitude to map moisture and/or cracks, to detect internal deficiencies or constituents such as cavities and/or reinforcement, to identify different building materials and to determine their depth and/or thickness [26–32]. Moreover, the combined use of GPR and IRT techniques in the inspection of historical buildings proved to be effective in obtaining detailed and valuable information (e.g., moisture content at different depths, corrosion, cracking, etc.) [33–38].

Recent publications have demonstrated the potential for integrating multi-source data into BIM in order to achieve a more complete and documented 3D modeling. Even though there are several studies using UAS or TLS data as a basis for BIM modeling [39–48], only a few published works integrate inspection methods, such as IRT and/or GPR data, into a BIM model [49–55].

This article presents the main results of the project "Heritage-3DIM: Modeling and Monitoring Cultural Heritage with 3D Geospatial Data", supported by the Institute for Systems Engineering and Computers of Coimbra (INESCC), aimed at developing an approach for integrating the results of several surveys into a BIM model. The employed methodology (Figure 1) includes different NDT techniques for both external (outdoors and indoors) and internal (through-the-thickness) characterization of the structure and its elements. It was applied to the masonry main façade of the Monastery of Batalha (Batalha, Portugal), combining two main types of information: (i) everything that characterizes the 3D as-is structure, such as geometry and materials, and (ii) the anomalies which presently affect the structure or its materials. The external surface geometry and its spectral properties were determined using a camera mounted on an UAS. The visible pathologies of the façade were also identified from RGB (red, green, blue) imaging. To complement this information, a GPR system was employed to examine the façade interior (through-the-thickness) while IRT was applied to the nearest sub-surface. All the gathered information, properly georeferenced, was fed to a 3D model obtained by a TLS technique and supported by a BIM model elaborated in Autodesk Revit. Information obtained with other techniques (either NDT or more intrusive) can obviously also be integrated in this BIM model.
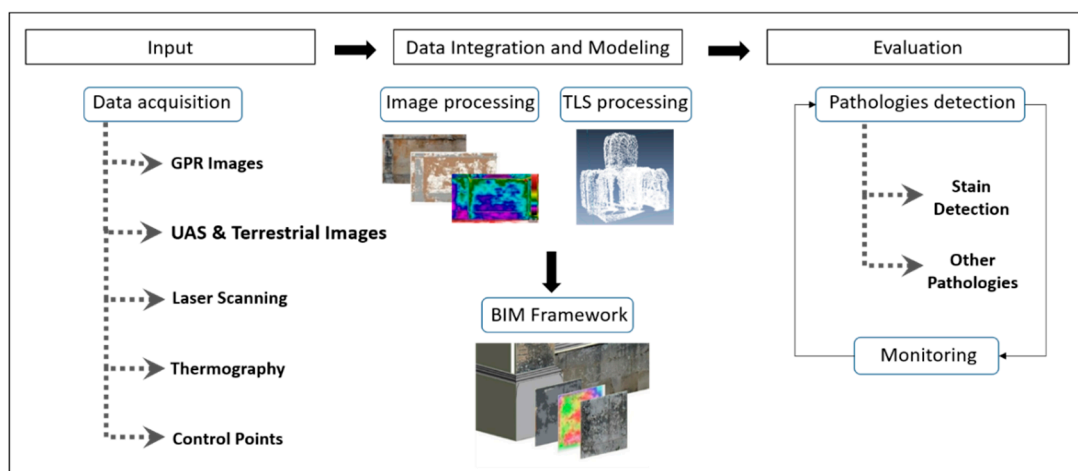

Figure 1. General overview of the methodological approach employed in the project "Heritage-3DIM: Modeling and Monitoring Cultural Heritage with 3D Geospatial Data".

It should be emphasized that our proposal is to demonstrate that (i) datasets having diverse origins, and even nature, can be effectively included in a unique BIM model, and (ii) such a concentration of information can assist future users in obtaining a general 3D display and interpretation of the building and its condition at a given time. Note, however, that the paper does not cover the automatic extrapolation of additional information from the hosted information.

This paper is organized into six sections: (i) Section 2 provides a brief description of the Monastery of Batalha and the zone selected as the case study; (ii) Section 3 deals with the surveying techniques employed for characterization, diagnosis and generation of the 3D model, including the description of methodologies used for data acquisition and processing; (iii) Section 4 shows and discusses the results of these surveys; (iv) Section 5 presents the approach followed for data integration into a BIM model; (v) Section 6 summarizes the main conclusions.

2. The Monastery of Batalha

The Monastery of Batalha (MB), also called Monastery of Santa Maria da Vitória, is located in Batalha, Leiria, in the center of Portugal. It is inscribed on the UNESCO World Heritage List and its main styles are Gothic and Manueline, a Portuguese late gothic. The main part of the monastery, which is being covered by the present research, was built under Master mason Afonso Domingues between 1388 and 1402 and then under Master mason Huguet, who was responsible for the Founder's

Chapel, until 1438 [56]. But new parts were added to the monastery (and others underwent important modifications) until 1530. From then until the beginning of the 19th century almost only conservation and restoration works were carried out. Between 1840 and 1900 the monastery suffered a significant intervention, which included the demolition of some parts, rebuilding some severely damaged elements, lowering by 65 cm the exterior pavement adjacent to the main (west) entrance, and also introducing some modifications to emphasize the gothic nature of the building, a regrettable practice of that period [57]. More recently, in the 1940s, another noteworthy intervention project took place.

The monastery was built with a compact sublithographic oolitic limestone (Bathonian stage) from the region [58]. Even though the intent in the 19th century rehabilitation intervention was to use the same material, different types of limestone, also from the region but weaker, were employed. As explained below in the results section, the GPR survey detected two different types of ashlar: one (probably) original and another one much more recent (probably applied in a restoration intervention). Unfortunately, there is no precise information about the type and date of application of the ashlars in the different parts of the monastery.

To assess the capabilities of each technique and to assure the representativeness of the gathered information, different parts and construction elements of the monastery were examined, namely (i) part of the monastery west façade, including some of its protruding buttresses, and (ii) some masonry vaults of the Church (nave, right-hand aisle and transept) and of the Founder's Chapel (see Figure 2). The west façade comprises three blocks of the monastery: the western aisle of the Royal Cloister, the Church (including its main entrance) and the Founder's Chapel.
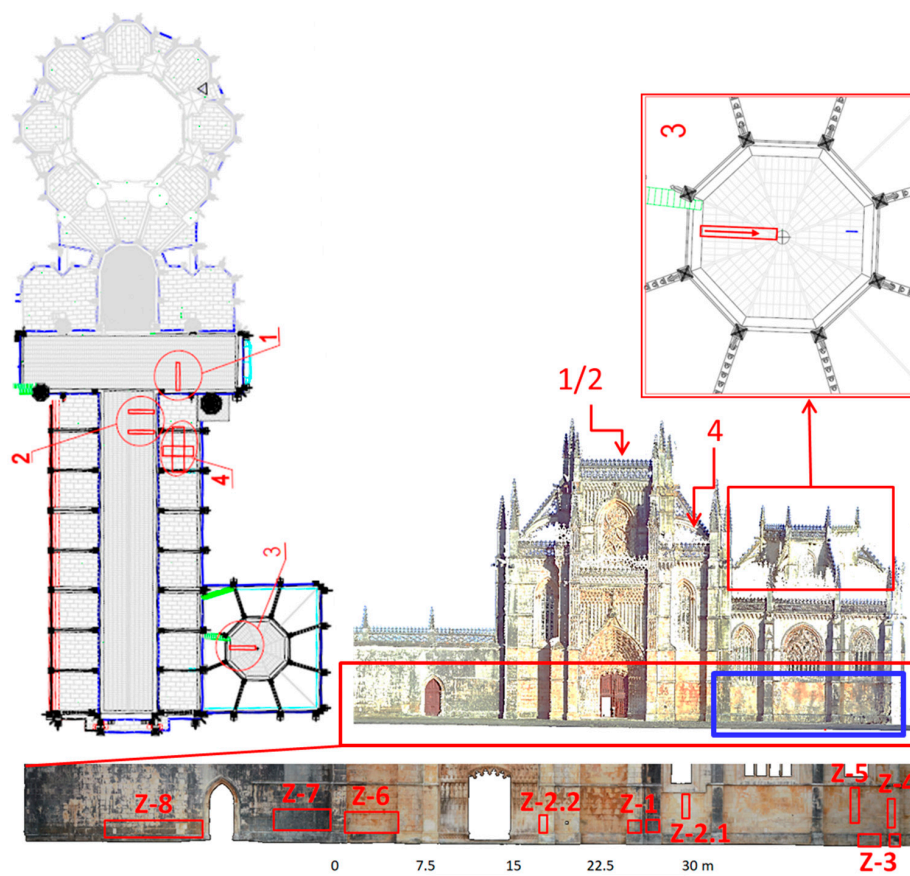

Figure 2. Orthoimage of the main façade of Monastery of Batalha (MB) with the zones prospected with ground-penetrating radar (GPR) (Z-7 and Z-8 correspond to the Royal Cloister, Z-1, Z-2.2, and Z-6 to the Church, and the remaining to the Founder's Chapel). The plan views depict the roof zones surveyed on the Church—transept (1), nave (2) and right-hand aisle (4)—and on the central part of the Founder's Chapel (3). The blue rectangle highlights the façade zone surveyed with infrared thermographic (IRT).

GPR and IRT surveys were performed on locations subject to past restoration interventions, in order to deepen our understanding of those interventions, which is required to improve future conservation and restoration plans. Moreover, the specific locations of GPR and IRT readings were chosen where better correlation with the characteristics of the façade could be obtained. In this sense, the GPR readings were made in order to obtain information about the internal structure of the different construction elements (such as walls, buttresses and roof). On the other hand, IRT was employed in the area where the classification of anomalies showed a larger variety (Figure 2).

Three buttresses of the main façade have been investigated: one stiffening the south façade of the Founder's Chapel, and the other two corresponding to the Church. The one closer to the right of the main portal is aligned with the arcade that separates the nave from the side-aisle (that supports the clerestory, see Figure 2), while the one further right corresponds to the Church's south wall (one part of it forming the exterior façade and the other being connected to the Founder's Chapel).

The interior spaces of the Monastery of Batalha are all covered by ribbed vaults. Most of them are quadripartite vaults but there are also a few stellar vaults: the latter type was employed in the inner octagonal center of the Founder's Chapel (exterior view in Figure 2). All these vaults are covered by fill materials and limestone tiles (or plates).

3. Materials and Methods

This section includes the geomatic techniques employed in the surveys. The BIM-based approach developed is presented as a separate section after the results of these surveys and the generation of the 3D model of the monastery.

3.1. Unmanned Aircraft System (UAS) Survey: Methodology for Façade Orthophoto Generation

In this study, the UAS and their payload RGB cameras are synergistic used as a cost-effective and innovative inspection method that allows the assessment of the state of conservation of existing heritage structures and enhanced efficiency in damage classification. The orthophotos generated by processing the imagery obtained by the UAS and object-based image classification methods will support the automatic identification of the anomalies on the facades and rooftop of the heritage buildings, where access cannot be gained without the installation of a heavy, complex, expensive and time-consuming scaffolding.

The orthophoto of the main façade of MB was generated using an SfM (structure from motion) and multiview stereo (MVS)-based approach. This orthophoto was generated in Photoscan Pro v1.4 (Agisoft LCC, St. Petersburg, Russia) by using four steps of the standard workflow, which is represented in Figure 3. In step 1, a block of 324 images of the main façade of MB was acquired using a multirotor UAS (Phantom 4 Pro, DJI, Shenzhen, China) and a vertical flight path (the white circles in Figure 3b represent the positions of the image centers). In step 2, the BBA (bundle block adjustment) of the image block was performed in an arbitrary coordinate system. For scaling the model, 18 distances measured in the CAD (computer aided design) drawing of the façade were used (Figure 3a). This CAD drawing, supplied by MB's administration, was previously generated by vectorising an old 3D point cloud obtained by laser scanning, in which an RMSE (root-mean-square error) of about 1.5 cm was obtained. The final accuracy of the adjusted scale was 2.8 cm. This value is given by Agisoft Metashape and represents the RMSE of the 18 differences between the input distances (measured in the CAD drawing) and the estimated values (computed in the scaled model). In step 3, a dense 3D point cloud was generated (Figure 3c). In step 4, this point cloud was used to generate a textured model and subsequently the orthophoto (Figure 3d).
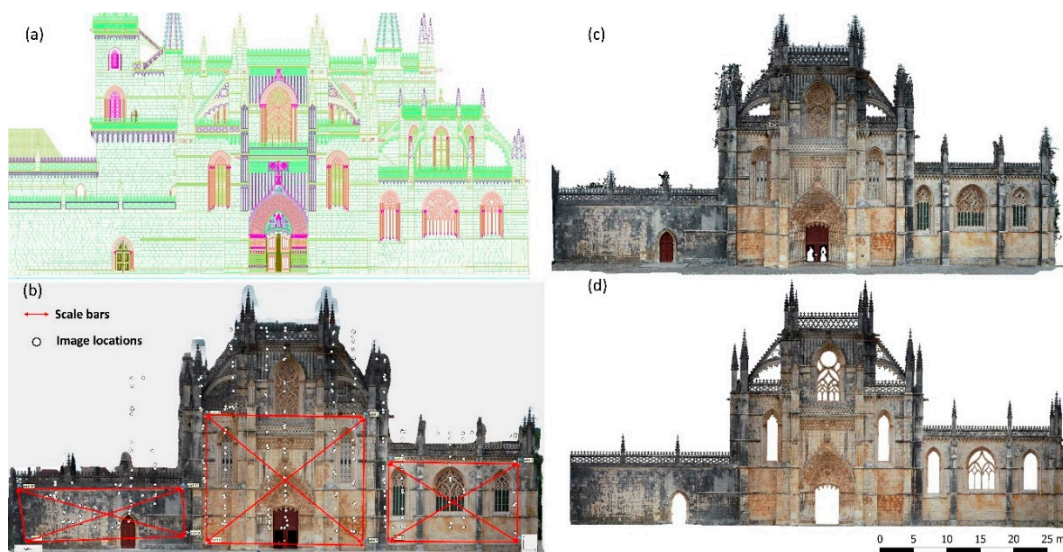
Figure 3. Generation of the orthophoto: (**a**) ancillary computer aided design (CAD) drawing used to scale the model; (**b**) location of the 18 scale bars and the 324 images acquired with a Phantom 4 Pro multirotor drone; (**c**) raw 3D point cloud generated by using an structure from motion multiview stereo (SfM-MVS) processing workflow on Photoscan Pro; (**d**) edited orthophoto with a GSD (ground sample distance) of 3.3 mm by using a textured model created from (**c**).

A visual inspection was then carried out to identify and classify the anomalies on the main façade of the monastery. Taking into account the spectral resolution of the camera employed and the properties of the stone-reflected radiation, the pathology types described in Figure 4 were selected.

Pathologies	Patina	Biogenic crusts	Sanding	Alveolization	Biologic colonization	Moisture
Nature	Chemical	Chemical	Physical	Physical Chemical	Microbiological	Environmental
Sample						
Color						
Class	1	2	4	5	6	7

Figure 4. Six main types of manually identified pathologies: patina, biogenic crusts, alveolization, sanding, biologic colonization and moisture.

Additionally, the automatic classification of the anomalies was performed using object-based image analysis (OBIA) and the k-nearest neighbor (KNN) classifier in the eCognition Developer v9.5 (Trimble GmbH, Munich, Germany) [59]. Image segmentation, the first step of OBIA classification, was undertaken using the multi-resolution segmentation algorithm with the following parameters: scale 65, shape 0.1, and compactness 0.4.

3.2. Ground-Penetrating Radar (GPR) Survey: Data Acquisition and Signal Processing

The GPR method was employed to assist in the characterization of the internal structure of the walls, piers, and roof, as well as to identify the different building materials, crucial information for investigating some of the detected pathologies.

As shown in Figure 2, eight zones (Z-1 to Z-8) of the main façade of MB were selected to be prospected with the GPR aiming to investigate the different building materials used for construction and reconstructions throughout history, namely to evaluate the use of recent stones, materials used in the buttress and the eventual connection with the main wall. Moreover, in order to evaluate different dome-filling materials, additional GPR measurements were carried out on the masonry roof of the

Church—transept (1), nave (2) and, at a lower level, right-hand aisle (4)—and of the octagonal central and higher part of the Founder's Chapel (3), above its stellar ribbed dome.

A ground-coupled pulsed system manufactured by Malå Geoscience© (Malå, Sweden) was used, composed of a Proex control unit and three different antennas with central frequencies of 500, 800 and 2300 MHz (Figure 5). The highest frequency provides greater resolution but lower signal penetration, while the lowest frequency provides poorer resolution but larger signal penetration. The setup used for data acquisition is summarized in Table 1. A survey wheel was attached to the antennas to control the trace-interval distance and measure the total length of the GPR profiles. Additionally, to guarantee positioning and accurate data integration, field marks were registered during data acquisition at the joints between stones.
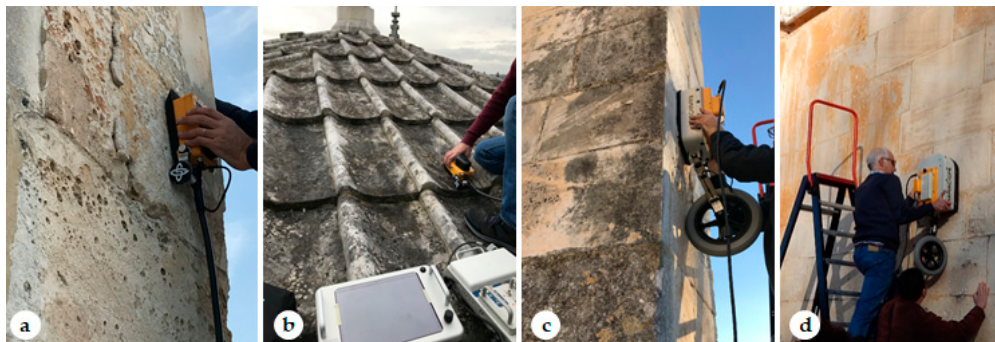

Figure 5. GPR system used for data acquisition and collection of GPR profiles through the main façade of MB (**a**) 2300 MHz antenna, (**c**) 800 MHz antenna, (**d**) 500 MHz antenna and roof of the Founder's Chapel (**b**).

Table 1. GPR acquisition setup.

Frequency	2300 MHz	800 MHz	500 MHz
Trace-interval (m)	0.01	0.01	0.02
Time window (ns)	15	35	75
Samples/trace	520	512	512

To enhance the extraction of information from the received GPR signals, they were first filtered and only afterwards the subsurface images with all interesting features were produced. The data was processed with the ReflexW software (Sandmeier geophysical research, Karlsruhe, Germany) [60] using the processing sequence described in Table 2. This filtering aimed to eliminate possible noise or interference with the signal, as well as to amplify the received signal (gain function) in order to mitigate possible losses or attenuations. To suppress the continuous component, a vertical or temporal filtering was applied (subtract-mean-dewow), determining and eliminating from each trace an average value based on the low energy of the last part of the wavelength. A horizontal or spatial filtering (background removal) was also applied to remove horizontal continuous low-frequency reflectors, which allowed estimating and removing an average value of all the traces in a time window. A band-pass filter (Butterworth) was then used to remove both low- and high-frequency noise in the vertical and horizontal directions. Finally, as presented in [61], migration processing (Kirchhoff) was used to suppress strong clutter aiming to improve the definition of the internal stone blocks.

To transform the travel-time distance (ns) axis of the GPR image into a depth/distance (m) axis, the radar-wave velocity was previously calibrated for the two types of found ashlars (as explained before): the original one and the much more recent one. This calibration was performed, as in [62], by considering the travel-time difference measured in the GPR signal and the actual thickness of the stone. The radar-wave velocities obtained were 13.4 cm/ns for the original stones and 11.4 cm/ns for the more recent ones, which resulted in an average radar-wave velocity of 12.4 cm/ns.

Table 2. Filters and parameters used for GPR data processing.

Filtering	2300 MHz	800 MHz	500 MHz
Time-zero correction	–	–	–
Dewow	0.44 ns	1.25 ns	2 ns
Gain function	Linear: 10 Exponential: 10	Linear: 2 Exponential: 2	Linear: 2 Exponential: 2
Background removal	–	–	–
Band-pass (Butterworth)	Low cut: 1600 MHzHigh cut: 4600 MHz	Not applied	Not applied
Migration (Kirchhoff)	Velocity: 12.4 cm/ns (summation width: 10)		

It is important to mention the technical difficulties experienced in data acquisition due to the excessive weighting of the antennas, especially with the 500 MHz antenna. As shown in Figure 5, a ladder was used to access the higher stonework of the façade and two operators were required in order to maintain both the GPR antenna and the survey wheel in permanent contact with the surface.

3.3. Infrared Thermographic (IRT) Survey: Thermal Image Acquisition and Processing

Infrared thermography (IRT) can be used for the investigation of historic structures, namely, to detect pathologies in the stone walls, during their heating or cooling phases, for example due to the presence of water that affects the surface temperature during the drying or wetting, or due to possible changes in the thermal diffusion of the wall [63].

The infrared images were captured with a thermographic Flir T335 camera (Flir Systems, Täby, Sweden). The inspection was carried out on the west façade of the Founder's Chapel (region highlighted in a blue rectangle in Figure 2). The capture of each single image was done as parallel as possible to the façade. Each single image was captured positioning the camera as perpendicularly as possible to the façade. The passive technique was used, profiting from the building façade heating or cooling according to the period of the day. Since the façade under study is facing west, the infrared images were taken in the morning to obtain acceptable weather conditions, when there was no direct solar radiation on the façade surface, avoiding heterogeneous heating of the stone.

3.4. Light Detection and Ranging (LiDAR) Survey: Data Acquisition and Processing

Light detection and ranging (LiDAR) scanning can be used to produce highly accurate 3D data and is becoming increasingly important for cultural heritage preservation, to capture building interiors [64] and provide digital documentation and deformation analyses of buildings [65–67]. Indeed, laser scanning captures the real condition of structures and its data can be used to create true as-built BIM models that can be relied on by engineers, architects, and contractors.

A tripod-mounted Faro Focus 3D X330 (Faro Technologies Inc., Stuttgart, Germany) [68], which is a phase-based TLS operating a laser of wavelength 1550 nm with an effective range of 330 m, was used for data acquisition (Figure 6a). A total of 58 scans were recorded in a complex geometry in the presence of occlusion. To capture the main façade of the monastery and the Founder's Chapel, 12 scans were performed outdoors and due to different object-to-scanner distances (ranging between 5 to 10 m), the computed surface density varies between 81, 428 to 20,285 points per square meter (pt/m^2). The remaining 46 scan positions were taken inside the Founder's Chapel, generating point clouds with a spatial resolution of 7 mm.

The point clouds from each scan were initially represented in the scanner's local coordinate frame. All the data were then aligned in a common, global coordinate system through a process known as registration (Figure 6b). For this purpose, plane targets fixed in common surfaces were used as control points in the Faro Scene software (Figure 6a). Besides, points on the floor were also coordinated in a local datum with a Global Positioning System (GPS). The Faro Focus 3D X330 was positioned on

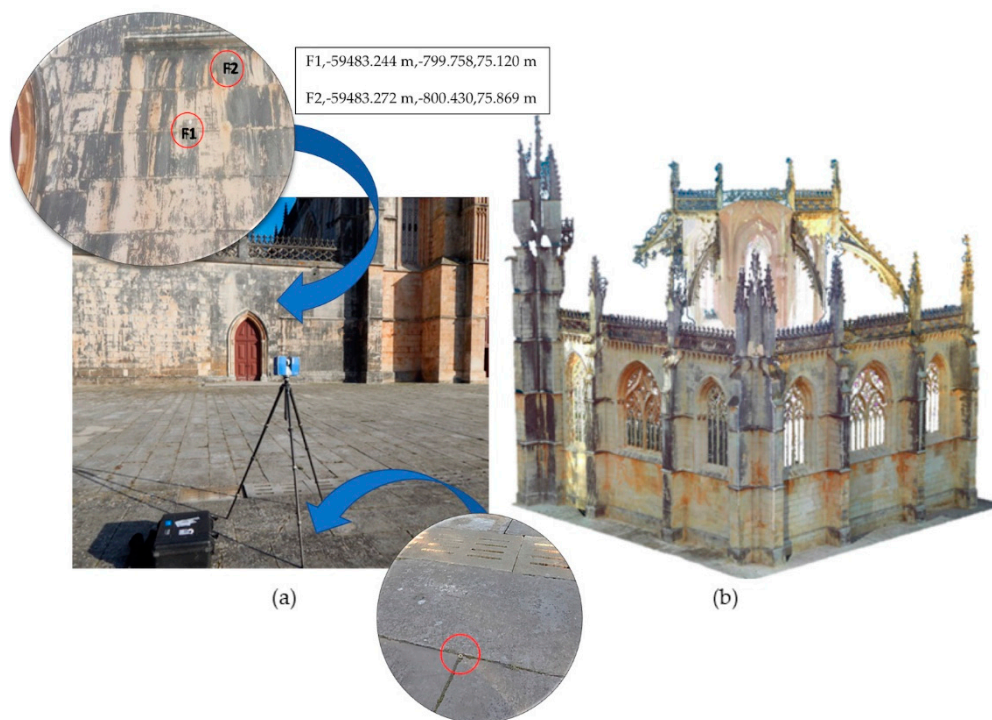these coordinated points to perform the point cloud surveys. This procedure yields a georeferenced 3D model.

Figure 6. (**a**) Faro Focus 3D X330 during data acquisition, and (**b**) Founder's Chapel point clouds after registration.

4. Results and Discussion

This section includes the individual results obtained from the surveying techniques. The integration of the data into a BIM is presented and discussed in Section 5.

4.1. Results of the Anomalies Classification

The main aim of the process was to compare the results obtained from the classic visual inspection with an automatic procedure, and the level of degradation in some cases was defined based on the difference of the colors. The method allows us to obtain a quantification of the area affected by a certain pathology and, if repeated over time, the evolution in terms of area affected. Due to the low spectral resolution of the camera and the reflected radiation properties of the stone, only two of the six types of anomaly of Figure 4 could be automatically identified: patina and biogenic crusts. Actually, different severity levels of patina and biogenic crust stains can be distinguished, so that each of them is subdivided in two subclasses: patina 1 and 2 and biogenic crusts 1 and 2. For instance, patina 1 is the severest or more advanced (having a darker tone) while patina 2 is still in an initial state (lighter tone)—biogenic crusts were similarly classified. By visual inspection of the orthophoto, a stratified random sample of 358 points was manually identified and used for training the supervised KNN classifier (with 5 nearest neighbors). Figure 7a shows the classification results of façade pathologies obtained by the KNN classifier. These automatically identified pathologies are in agreement with the pathologies identified manually by the visual inspection of the façade orthophoto (Figure 7b), which took 104 h for an experienced operator.

For assessing the accuracy of the OBIA classification, a stratified random sampling was used (Table 3). The overall accuracy of the automatic classification was high (76.5%) with a moderate agreement among the automatic classification and the reference data, given by a kappa coefficient $k = 0.71$. The producer's accuracy (pa) was lowest for class patina 2 (59%) and highest for patina 1

(88%) and the no pathology class (87%). The user's accuracy (ua) showed higher values for biogenic crusts 1 and 2 (respectively 92% and 84%) and much lower values for patina 1 (59%).
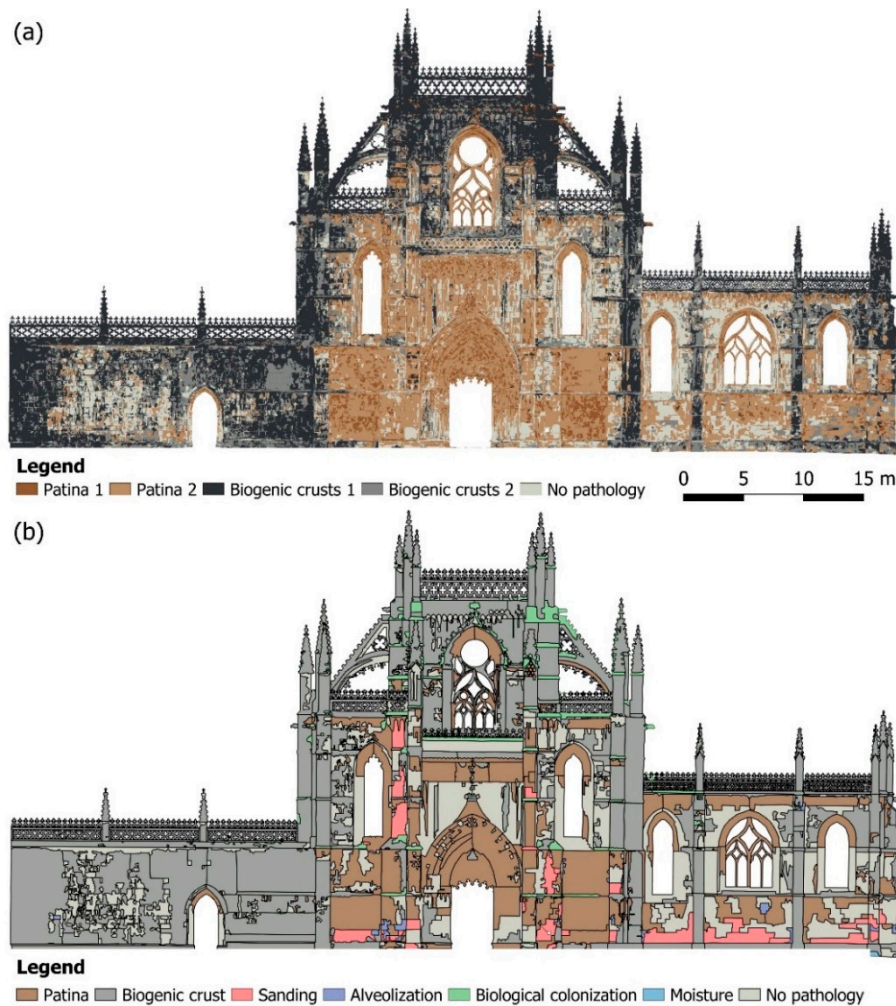

Figure 7. Classification of anomalies on the main façade of MB: (**a**) automatic classification based on object-based image analysis (OBIA); (**b**) manual classification based on visual inspection.

Table 3. Error matrix and associated OBIA classifier accuracy based on 289 stratified random samples. Pt1 = patina 1, Pt2 = patina 2; BCr1 = biogenic crusts 1; BCr2 = biogenic crusts 2; NP = no pathology; Ua = user's accuracy; Pa = producer's accuracy; Oa = overall classification accuracy; k = kappa coefficient.

	Pt1	Pt2	BCr1	BCr2	NP	Ua
Pt1	38	24	2	0	0	59%
Pt2	5	44	0	5	5	75%
BCr1	0	1	47	3	0	92%
BCr2	0	2	7	52	1	84%
NP	0	3	1	9	40	75%
Pa	88%	59%	82%	75%	87%	
Oa = 76.5%; k = 0.71						

One of the advantages of using a super high-resolution orthophoto for mapping the façade pathologies is that it is possible to evaluate, in a simple and direct way, the area occupied by each (Table 4).

Table 4. Comparison of the areas occupied by each pathology. Pt1 = patina 1, Pt2 = patina 2; BCr1 = biogenic crusts 1; BCr2 = biogenic crusts 2; NP = no pathology; Sd = sanding; Av = alveolization; BCo = biologic colonization; Ms = moisture.

Pathologies	Manual Classification		Automatic Classification	
	m^2	%	m^2	%
Pt1	278.05	21.65	74.94	5.85
Pt2			354.52	27.67
BCr1	658.66	51.29	421.17	32.87
BCr2			239.34	18.68
NP	264.08	20.56	191.34	14.93
Sd	39.16	3.05	-	-
Av	4.71	0.37	-	-
BCo	36.83	2.87	-	-
Ms	2.64	0.21	-	-

The values presented in Table 4 allow is to conclude that about 51% of the study area presents biogenic crusts and the area values identified with both methods are very similar (automatic classification—660.51 m^2, manual classification—658.66 m^2). Concerning the areas presenting Patina, a difference of about 37.6% was obtained between the two methods.

4.2. Interpretation of the Produced GPR Images

Figure 8 presents the radargrams obtained along the eight different zones (Z-1 to Z-8) of the main façade of MB (see Figure 2). First, Figure 8a presents the data produced with the 500 MHz antenna in Zone 1 (façade buttress). Three different depths of the inner surface of the ashlars are identified: the first at ~80–100 cm, the second at ~150–170 cm and the third at ~240–280 cm. Second, Figure 8b shows the 2300 MHz data obtained in Zone 2.1 (wall below lancet window of Founder's Chapel), while Figure 8c illustrates the 2300 MHz data produced in Zone 2.2 (buttress at the end of the arcade separating the nave from the right-hand aisle), showing the interpretation of the different stone's thicknesses. As seen in Figure 8b, a cavity (wall tomb) in the internal skin of the façade at Zone 2.1 causes (red ellipse) signal diffractions and complex pattern of reflections at the end of this profile (from 1.4 to 2.2 m), which were certainly produced by the cavity (gap) and the limestone arch above the internal wall tomb, respectively. Next, observing the 2300 MHz profile produced in Zone 3.1 (Figure 8d), it was realized that the bottom row of ashlars on the façade was recently restored using a stone ~10 cm thick; whereas observing the profile acquired in Zone 3.2 (Figure 8e), it was inferred that the second and third rows (from the bottom of the wall) are composed of the original stones ~50–60 cm thick. Figure 8f includes the radargram obtained with the 2300 MHz antenna in Zone 4, where both the original ashlars (thickness ranging from 40 to 70 cm) and those used in recent restoration interventions (thickness ranging from 2 to 12 cm) are detectable on the stonework of the façade. The thickness variation observed for a singular type of material is almost certainly caused by defects such as alveolization or by the unevenness of the inner face of the ashlars. Figure 8g presents the radargram obtained with the 2300 MHz antenna in Zone 5. As in Zone 4, it was possible to observe the presence of both original (~35 cm thick) and new (~8–10 cm thick) ashlars, the latter used for restoration. Regarding Zone 6, Figure 8h illustrates the radargram produced with the 500 MHz, showing three different layers of ashlar at ~60, 130 and 200 cm in depth. The reflection observed at 200 cm depth at the beginning of the radargram is most certainly produced by the wall separating the Royal Cloister from the Church, which is perpendicular to the surveyed façade. Figure 8i presents the radargram obtained with the 800 MHz frequency antenna in Zone 7. Observing these radargrams, a single layer of ashlars ~60 cm thick is identified. Finally, Figure 8j displays the radargram obtained with the 800 MHz frequency antenna in Zone 8, where both original (thickness ranging from 50 to 60 cm) and recent ashlars (thickness ranging from 5 to 10 cm) are distinguishable on the stonework of the façade.
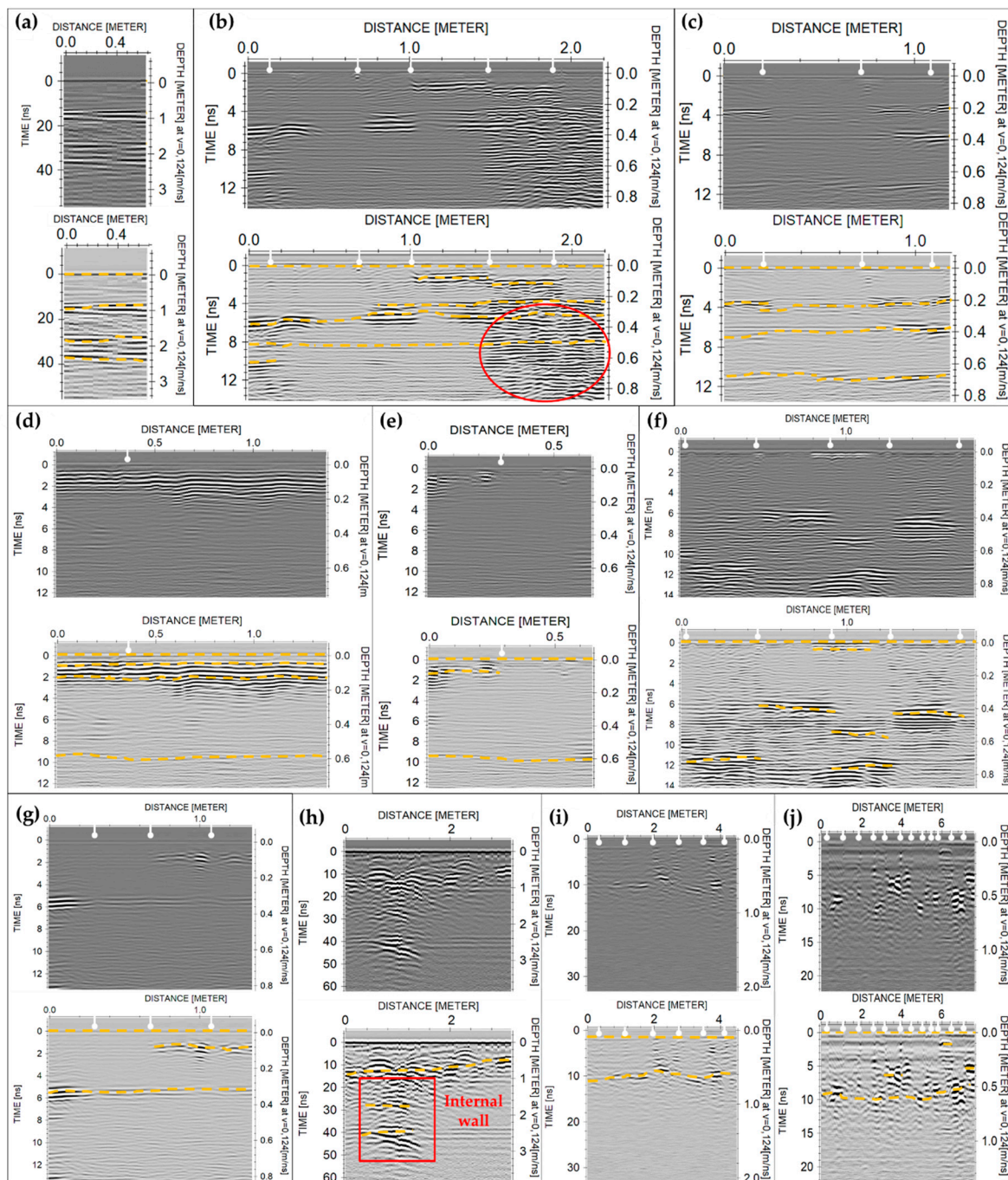
Figure 8. GPR data produced on the main façade of MB: (**a**) 500 MHz data in Zone 1, (**b**) 2300 MHz data in Zone 2.1, (**c**) 2300 MHz data in Zone 2.2, (**d**) 2300 MHz data in Zone 3.1, (**e**) 2300 MHz data in Zone 3.2, (**f**) 2300 MHz data in Zone 4, (**g**) 2300 MHz data in Zone 5, (**h**) 500 MHz data in Zone 6, (**i**) 800 MHz data in Zone 7, (**j**) 800 MHz data in Zone 8. (Vertical white marks are the field marks used for data integration, which corresponds to the separation of successive external stone blocks, while horizontal yellow dashed lines indicate the separation of successive internal stone blocks.).

Figure 9 includes the GPR data acquired on the roof of both the Church and the Founder's Chapel (see Figure 2). First, Figure 9a presents the radargram obtained with the 2300 MHz frequency antenna through the roof of the Founder's Chapel (Figure 8b), showing the interpretation of the superficial limestone tiles and stronger reflections at the internal fill layers. Regarding this effect, previous maintenance works carried out on the roof of the Founder's Chapel, in which some cladding tiles were

removed, revealed a fill layer made of lime mortar, stones and ceramic tiles. The scattering observed is certainly produced by the presence of such heterogeneous filling. Next, Figure 9b shows the radargram obtained with the 800 MHz frequency antenna on the roof above the right-hand aisle (second bay counting from the transept). It allowed for measuring the thickness of the cladding plates and of the internal fill layer (~20 cm and 80 cm thick, respectively), and to identify the top of the underneath ribbed vault (possibly its keystone). Finally, Figure 9c illustrates the radargrams obtained with the 800 MHz frequency antenna on the roof of the Church, above the nave and transept (see Figure 2), showing the cladding tiles and the internal fill layer.
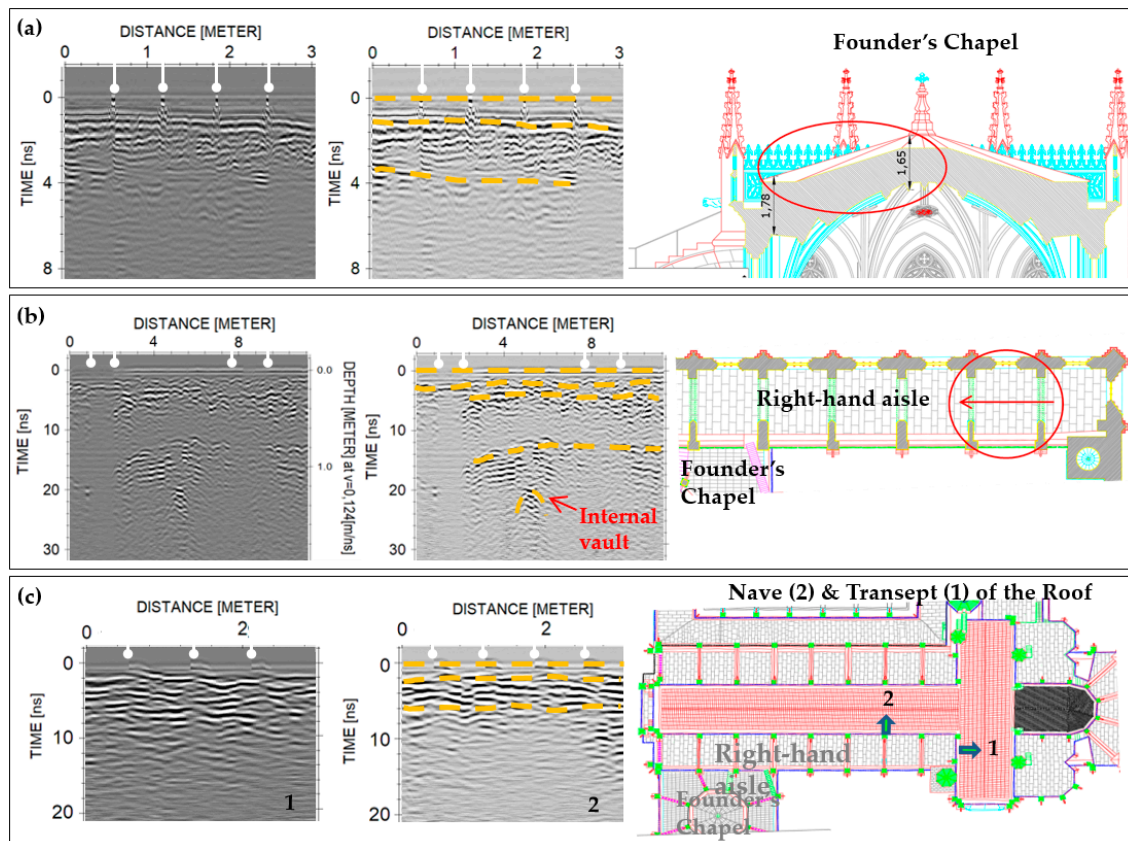

Figure 9. GPR data acquired on the roof of the Church and of the Founder's Chapel: (**a**) 2300 MHz data on the roof of the Founder's Chapel, (**b**) 800 MHz data on the roof above the right-hand aisle, and (**c**) 800 MHz data on the roof of the Church (above the nave and transept). (Vertical white marks are the field marks used for data integration, which correspond to the separation of successive external tiles, while horizontal yellow dashed lines indicate the separation of successive internal layers.).

4.3. Analysis of the Captured Thermographic Images

Figure 10 shows the images captured with the thermographic camera on the study area, and identifies the three wall spans t1, t2 and t3, bordered by the buttresses. Figure 10b shows the images captured on the wall span t3 (images P5 and P2) and bordering buttresses (images P1, P3, P4 and P6). In the areas closest to the ground (P1, P2 and P3) lower temperatures are observed (tones purple to blue in the thermogram), which are probably due to the presence of moisture, both absorbed from the ground (rising damp) and infiltrated in the façade, as confirmed by visual observation. The different colors are associated not only with different humidity levels but also with the material and pathology types–as they imply different absorption of solar radiation and, therefore, different energy emissions captured by the thermogram–and with the thickness of the limestone blocks. There seems to exist some match for areas with patina and also in the presence of stones resulting from recent restoration works in the upper middle part of P5 (Figure 10). In addition, higher temperatures (reddish

color) are observed (1) near the pier buttresses, on the left-hand side of P5, which appear to be caused by the presence of the buttress, and (2) on the frieze at the top of P5, close to the window sill.
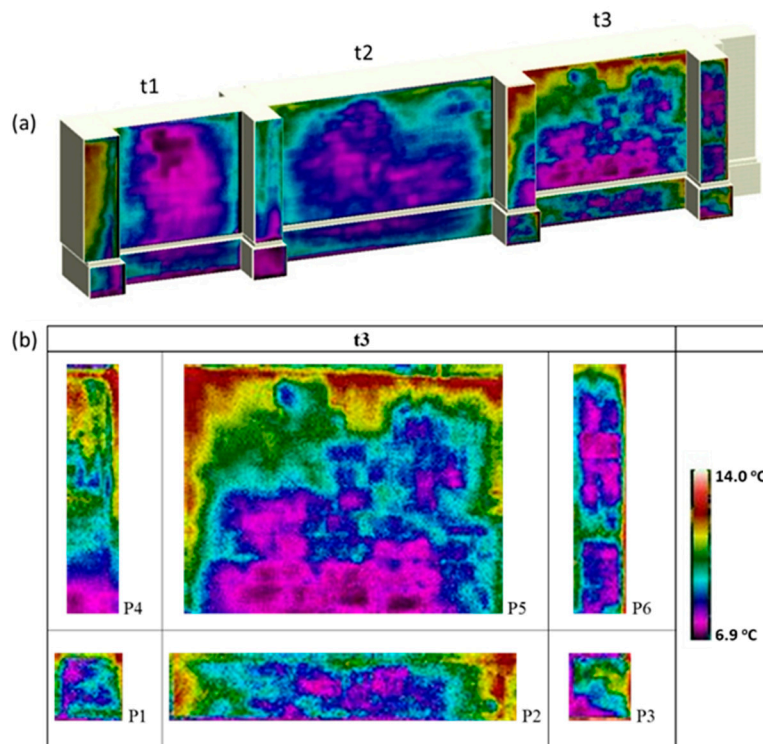

Figure 10. Infrared thermography of the study area: (**a**) areas t1, t2 and t3 of the Founder's Chapel; (**b**) thermographic images for area t3.

4.4. Three-Dimensional (3D) Model Generation and Structural Analysis

To create the 3D model the raw point clouds were first converted to a readable project file (RCP), using the Autodesk ReCap (San Rafael, CA, USA), which was then imported to a BIM environment using the Autodesk Revit software. The large amount of data contained in the indoor and outdoor point clouds allowed the actual dimensions of the surveyed walls and piers of the Founder´s Chapel to be determined, and subsequently to be introduced in a BIM Platform (Figure 11). In addition, the point clouds were also used to evaluate the inclination of the inner columns of the Founder´s Chapel and therefore the deviations and alignments of the chapel.
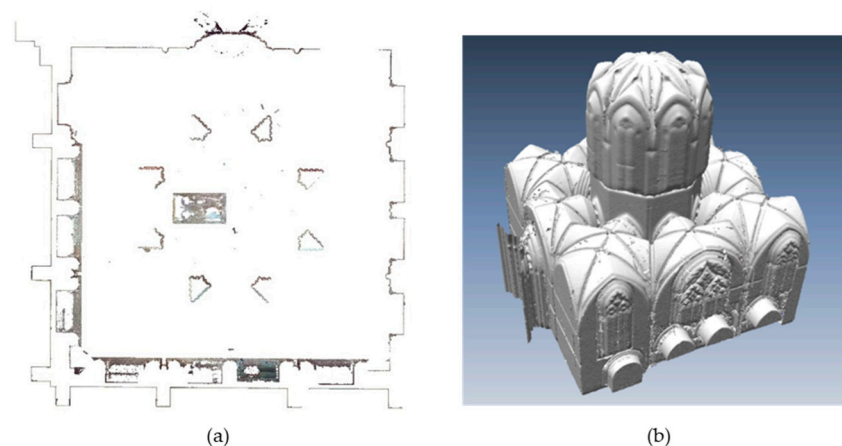

Figure 11. Founder's Chapel: (**a**) floor plan view in Autodesk Revit, (**b**) 3D model after indoor cloud registration.

The interior of the chapel was analyzed according to 8 vertical alignments corresponding to the 8 central columns of the Founder's Chapel, located between the windows of the octagon at the roof level. The coordinates of four points were taken in each vertical alignment at 3.7 m, 12.7 m, 13.6 m and 16.5 m from the floor (see Figure 12). In this figure, the lower level (3.7 m) dimensions are in natural scale and the others have a factor scale increase of 20 with respect to the coordinate difference to that lower level. The figure shows that the Founder's Chapel presents at its higher level a displacement to the south (maximum of 11.4 cm), east and west (maximum of 8.2 cm) sides, possibly due to misalignment during the construction stage or in consequence of seismic activity (the original roof collapsed during the Lisbon earthquake of 1755 [69]). The figure also shows that the part of the octagon on the side of the Church suffered smaller displacements possibly because of the structure's higher stiffness in that direction (it may even have been pushed away from the Church by its horizontal impulse). The results show an average column inclination of about 8 mm/m. These displacements are probably the main reason for the open joints above the windows. It is possible that either the roof collapse due to the earthquake of 1755 or the construction of the new roof may have worsened the octagon deformation. By comparing the results of future surveys with those now obtained, it will be possible to determine if this motion is still evolving or if it has already stabilized.
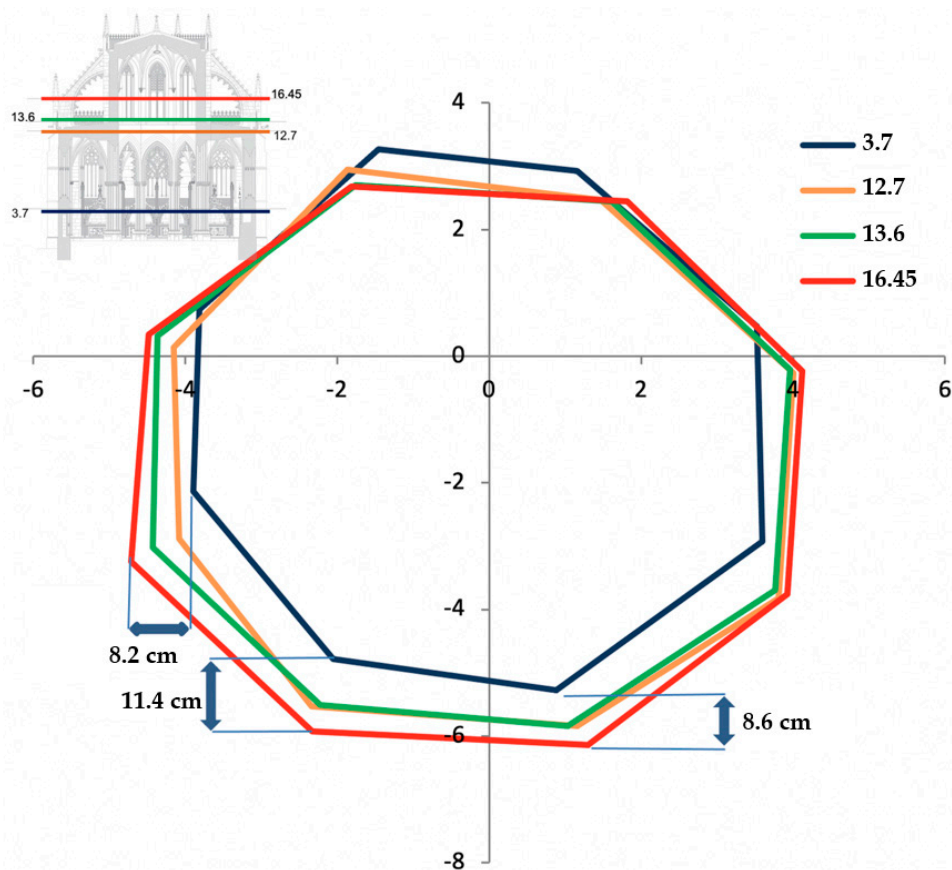

Figure 12. Horizontal displacement at four different levels (3.7 m to 16.45 m) of the star vaulted octagon of the Founder's Chapel.

5. Data Integration into the Building Information Modeling (BIM) Model

This section describes the steps followed to merge into a BIM environment the geospatial data presented in the previous section, as well as the optimization and treatment of those data. The main objective is to make this model available for possible uses in the future, such as facility management, support to conservation activities, rehabilitation interventions, or further research.

5.1. Methodological Approach for Data Integration

As mentioned in the previous section, as a first step of the development of the BIM model in Autodesk Revit, the LiDAR point clouds file (RCP) was imported into the BIM environment, and used to create the 3D walls of the façade, with the dimensions defined by the point clouds. In keeping with the object-oriented approach of BIM, this involved the creation of an initial wall object which was subsequently replicated by adjusting its properties. A similar approach was followed with the buttress piers (see Figure 13). In spite of the existence of several libraries of building elements in the Revit platform, specific objects had to be created for this project, such as the object walls, and the coating materials and their characteristics had to be introduced in the corresponding database.

Figure 13. (**a**) Three-dimensional view of the wall object of the façade, (**b**) plan view of the point clouds superposed to this wall object.

To overcome the lack of interoperability between the software used to produce the classification map (eCognition Developer v9.5) and the Autodesk Revit (San Rafael, CA, USA), all the information was saved in JPEG format, which is supported by the software. Only afterward was the remaining information successively inserted into the model: the orthophoto images obtained with the UAS, the radargrams, the IRT images and the pathology classification maps (Figures 14 and 15).
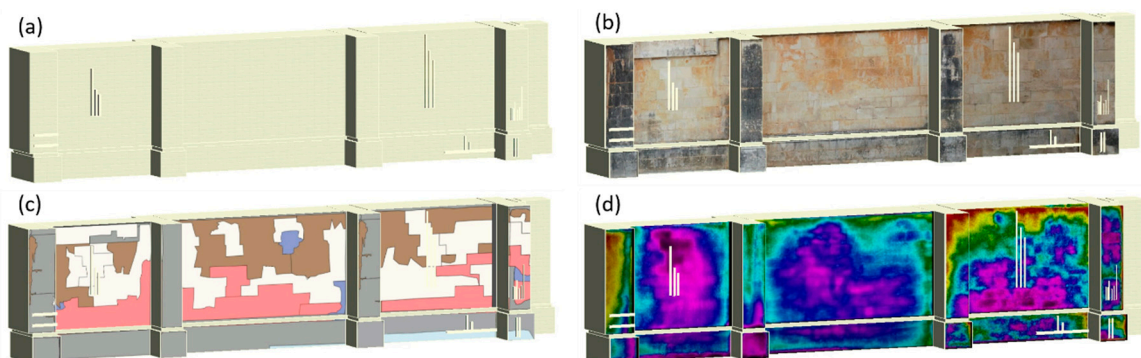

Figure 14. Three-dimensional model of the bottom part of the chapel façade with (**a**) location of the radargrams, (**b**) orthophoto image obtained with the unmanned aircraft system (UAS), (**c**) OBIA classification map and (**d**) thermographic image.

Figure 15. Images and maps on the bottom part of the chapel façade integrated in the BIM model.

Since this remaining information was georeferenced in an arbitrary coordinate system, all the information was co-registered inside the model using the dimensions defined by the point clouds or coordinates of common spatial elements (edges and corners), which are easily identifiable in the parametric model.

The strategy devised to integrate all the information into the model with their precise location and orientation was twofold: (i) the orthophoto images, the pathology classification maps and the IRT images, which are exterior information, were overlaid upon the model as wall and column claddings in a 3D plane, with the dimensions defined by the point clouds, while (ii) the GPR radargrams were positioned in the BIM 3D model using the field marks at the joints of the stones with their positions visible on the orthoimages.

The main difficulties found in these operations were caused by (i) the exterior wall and column surfaces pertaining to different plans and (ii) Revit software not allowing the simultaneous cladding of several coatings as different layers. To overcome these obstacles, a two-step procedure was conceived. First, the overlaid images and maps were cut out with the dimensions of the surfaces of those elements to which they were to be applied, to allow their insertion in the BIM model as coatings. Secondly, a virtual wall was generated for receiving each image or map as a coating, with all these virtual walls in the same position, and corresponding to the unique real wall. This solution allows the visualization of all images and classification maps in a unique BIM model, enabling their comparison and analysis (Figure 15).

To include the GPR radargrams in the model with their actual direction, position and dimensions, several possible solutions were tested. The chosen one was to create for each radargram a fictitious wall-object belonging to the Revit wall family. Each of these Revit wall objects was then cladded with a radargram. This allows the visualization of the radargrams by simply hiding the façade wall (Figure 16a). As an example, Figure 16b shows the 2300 MHz radargram corresponding to Zone 2.1 positioned in the BIM model.
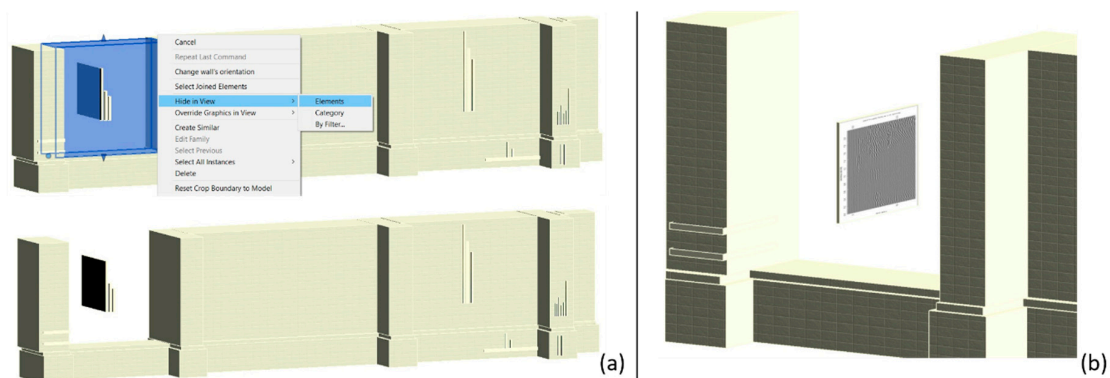

Figure 16. Revit model showing an existing panel of the façade of the Founder's Chapel containing a fictitious wall object cladded with a radargram: (**a**) visual disclosure of the radargram by hiding the wall using the Revit command "Hide in view", and (**b**) visualization of the radargram (cladded to a fictitious object).

Another challenge was the inclusion of the metadata information associated with each radargram, orthophoto images, IRT images and the pathology classification maps. For example, for each radargram a fictitious wall-object belonging to the Autodesk Revit wall family was defined. But there is some more relevant information, the so-called metadata, such as how was that radargram was produced, what equipment was employed, what were the antennas' characteristics, etc. In fact, this metadata is required to better document each radargram and exploit its potential and integration in the main model, and also for correlation with future information. When a "BIM Family" object is added to a project 3D parametric model, the latter can be enriched with more information contained within the inserted object. This information can, therefore, be interrogated, edited, and updated later on. Thus, for each new BIM family created within the "Identity" parameter type, the corresponding information was associated, such as a brief description of the data, the survey date, the equipment used, the person responsible for producing the information, or a URL link with supplementary technical information. In addition, files in PDF format were also added with technical details and the attribute "Comment" filled with the main characteristics or analyses of each object to allow their access directly through the properties panel (Figure 17).
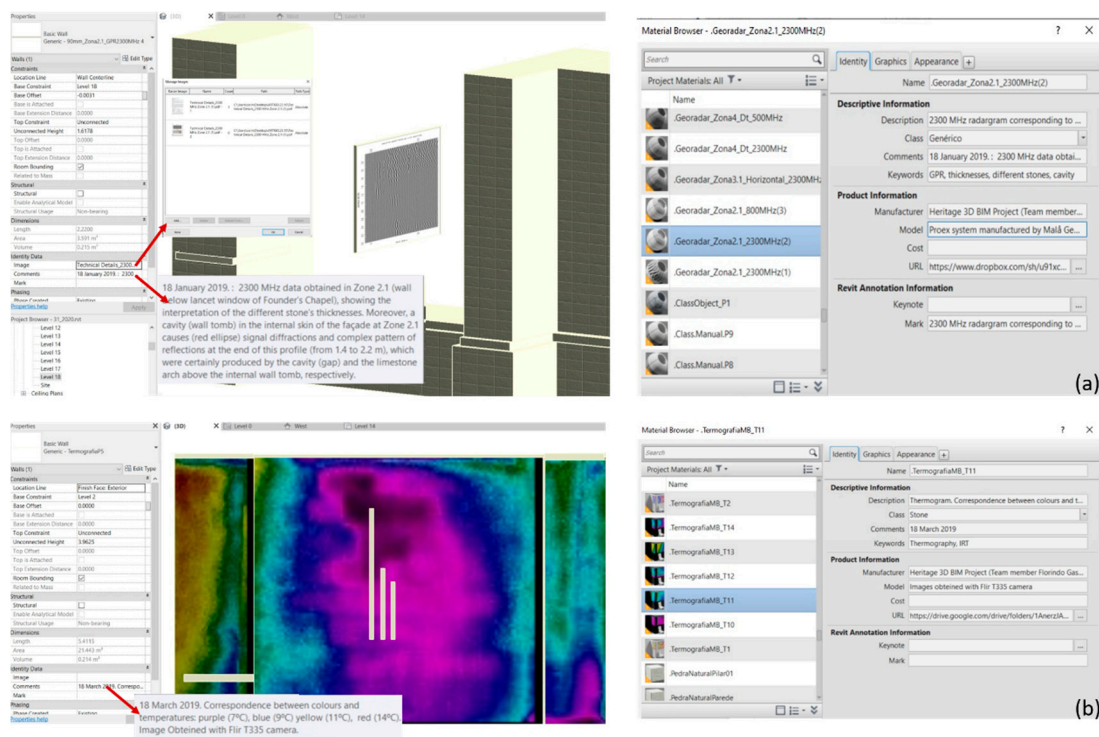

Figure 17. Revit database information associated to (**a**) the 2300 MHz radargram corresponding to Zone 2.1 and (**b**) the infrared thermography images.

In brief, the Autodesk Revit platform used proved capable of easily receiving all the information, i.e., the images obtained from the surveys, the maps with the classification of anomalies and some corresponding metadata information, allowing its integration and visualization. Using a collaborative platform, like Autodesk360 (San Rafael, CA, USA), it is possible to share and visualize the model, as well as to access the associated information or link handover information from a web browser. In addition, the created model and objects can also be exported as IFC (Industry Foundation Classes) files. Nowadays, IFC is widely recognized as the leading interoperability standard and Autodesk supports buildingSMART, the organization that develops and maintains the IFC standard for both buildings and civil infrastructure allowing an opening collaboration between professionals.

With respect to the integration of the different types of captured data, the radargrams were revealed to be the most challenging but, as described above, the creation of fictitious walls perpendicular to the

surveyed façade (and which may be imagined as drawers in this façade), overcame all the integration difficulties and turned out to be the method that best suited these through-the-thickness records.

Conversely, the BIM approach has a major drawback since "historical" buildings are often composed of "non-standard" elements. Thus, despite the existence of several libraries of building elements in the Revit platform, historical buildings require the creation of new architectural elements, namely "new component families", which is an extremely time-consuming task.

5.2. Integrated Data Interpretation

Figure 18, respecting the Founder's Chapel façade, illustrates a possible analysis of the combined representation of the OBIA classification, IRT and GPR imaging, showing the potential of the integration of data captured with different sensors (different ranges of penetration) into a BIM model (spatially overlapped). The areas highlighted with red circles can be interpreted as "anomalies" (different distribution of temperature, different time of reflection, etc., when compared with the surroundings). By analyzing the different information for the areas P5 and P6 of section t3 (see Figure 10), it may be concluded that zones with stones introduced during recent restoration works might show a lower temperature (IRT) and lower thickness of the blocks (GPR) and a "no pathology" status in the automatic classification. Also, regarding the central wall in section t1, the area having the lowest temperature (highlighted with a red circle) matches spatially the cavity detected with the GPR. Thus, the wall is less thick at this point, which corroborates that smaller thicknesses were associated with lower temperatures.
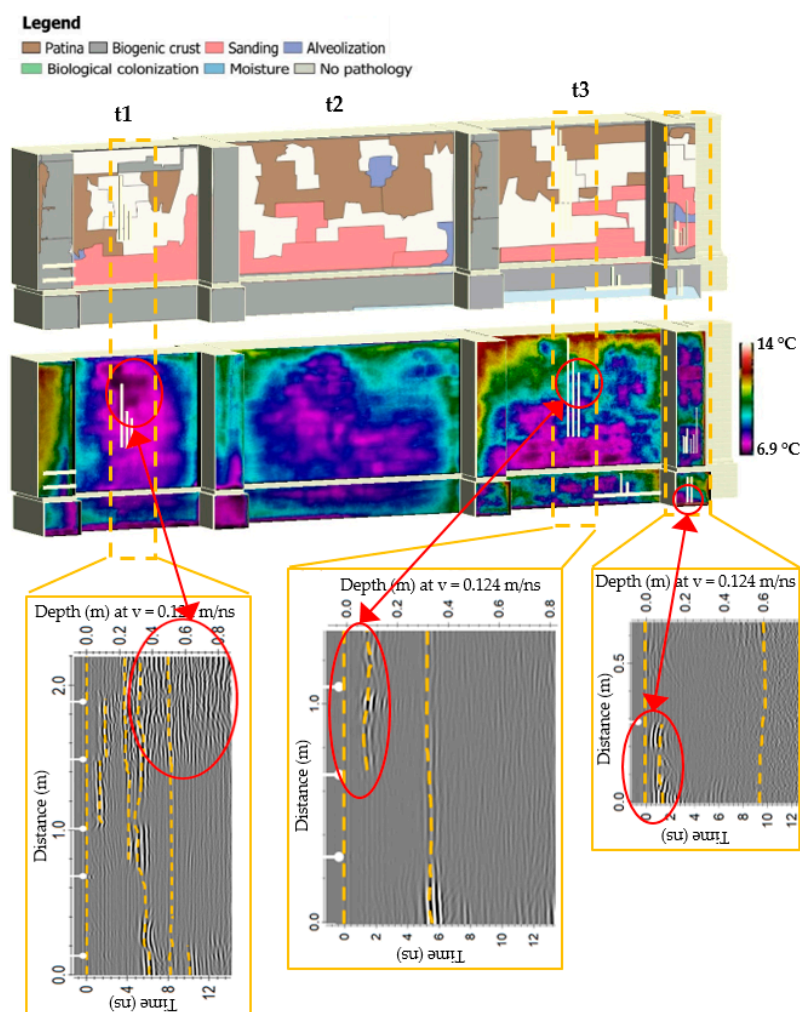

Figure 18. Analysis of the combined representation of the OBIA classification (UAS imaging), IRT and GPR results: the areas highlighted with red circles can be interpreted as "anomalies".

The proposed approach allows the integration of all the information obtained with several non-destructive techniques in a unique platform, proving the benefits in terms of interpretation and analysis and its usefulness in supporting and preserving built heritage data and documentation.

6. Conclusions

This work presents the results of a multidisciplinary survey for the inspection and characterization of some parts of the main wall façade of the Monastery da Batalha, a UNESCO World Heritage Site, using several non-destructive technologies: UAS, TLS, GPR and IRT. All the results produced were eventually integrated into a unique BIM model, providing a useful basis to permit their integrated analysis and interpretation. The most interesting findings from a diagnostic point of view were:

- The super-high resolution orthophoto obtained by the cost-effective UAS technology allowed the automatic identification of several pathologies and the area that each pathology occupies on the façade.
- The terrestrial laser scanning proved to be capable of generating a well-documented 3D model, as well as 2D plans, and the evaluation of the real condition of the structure, which plays an important role for heritage documentation purposes. It also permitted the tilt of the columns of the Founder's Chapel to be measured, a crucial information for assessing its stability.
- The GPR allowed determining the depth of the most superficial layers (of blocks) of the structure, detection of possible cracks, voids, variations of the depth or type of material of the blocks, etc. Moreover, the use of different frequency antennas (combining different resolutions and different depths of penetration) in the same zone sometimes led to additional information.
- The IRT information allowed detection of the presence of moisture, areas with patina and previous restoration works.

The proposed methodology intends to be a contribution to the application of the BIM approach to cultural heritage, aiming at the future use of the developed BIM model in different activities such as facility management, support in the restoration or rehabilitation processes and further research. Even though the development of a BIM model is a time-consuming task, it offers the ideal platform for the work and collaboration of multidisciplinary teams—however, in order to be truly useful, this model requires incessant updating and enrichment through additional information and data. The concentration of all the relevant information in a unique platform permitted by such a BIM model will strongly reduce the time required to access that information. Moreover, its visualization options, assisting in the interpretation of the requirements and results, the possibility of connectivity to other data systems and software, as well as the possibility of integration of simultaneous or non-simultaneous activities, also contribute to its added value.

In the study case presented, the integration in the BIM model of all the information obtained (the orthophoto images, radargrams, the maps with the classification of anomalies, thermographic images) was quite satisfactory. This integration and the visualization possibilities it offers will make this information easily available to support built heritage documentation and to assist in its preservation. The Revit platform proved to be capable of easily receiving all these additional non-standard types of information. The creation of the fictitious parallel walls perpendicular to the plane of the façade (the so-called drawers in the wall), turned out to be the method that best suits these through-the-thickness records and ultimately overcame all the integration difficulties. Furthermore, the set of collected images and the developed BIM model offer the possibility of creating a virtual reality (VR) environment which, thanks to hyper-realistic visual effects, can provide an accurate overall picture to every professional in the project team (architects, civil engineers, surveyors, mechanical engineers, contractors, conservators, etc.). Combining BIM and VR, the current state of the monument, as well as possible reconstruction or restoration alternatives, can be dynamically visualized, allowing end-users to interact with the virtual space and its components. In addition, a VR tour can be applied to a BIM model in order to check, from a facility management perspective, the maintenance schedule

(7D/BIM model), or from a project team view, the reconstructions review (4D/BIM model) supporting responsible decision making.

Finally, it is worth emphasizing that many questions remain in some fields covered by the present work. These start with how the information determined by each individual technology can be integrated and compared. There is a need to investigate ways to integrate the results obtained with each individual technique based on the spatial co-registration of technologies without placing marks/targets on the constructions, particularly in monuments, due to the visual impact and possible degradation of the surface. The integration of all the information generated along the monument's life is another huge challenge, which will require the definition of clear rules for modeling and recording information, so that it can be looked up and used by other stakeholders later on.

References

1. Vecco, M. A definition of cultural heritage: From the tangible to the intangible. *J. Cult. Herit.* **2010**, *11*, 321–324. [CrossRef]

2. La Russa, M.F.; Fermo, P.; Comite, V.; Belfiore, C.M.; Barca, D.; Cerioni, A.; De Santis, M.; Barbagallo, L.F.; Ricca, M.; Ruffolo, S.A. The Oceanus statue of the Fontana di Trevi (Rome): The analysis of black crust as a tool to investigate the urban air pollution and its impact on the stone degradation. *Sci. Total Environ.* **2017**, *593–594*, 297–309. [CrossRef] [PubMed]

3. Martín-Gil, J.; Martín-Gil, F.J.; Ramos-Sánchez, M.D.C.; Martín-Ramos, P. The Orange-Brown Patina of Salisbury Cathedral (West Porch) Surfaces: Evidence of its Man-Made Origin (5 pp). *Environ. Sci. Pollut. Res.* **2005**, *12*, 285–289. [CrossRef] [PubMed]

4. La Russa, M.F.; Ruffolo, S.A.; Belfiore, C.M.; Pogliani, P.; Pelosi, C.; Andaloro, M.; Crisci, G.M. Cappadocian ignimbrite cave churches: Stone degradation and conservation strategies. *Period. Mineral.* **2014**, *83*. [CrossRef]

5. Grossi, C.M.; Esbert, R.M.; Díaz-Pache, F.; Alonso, F.J. Soiling of building stones in urban environments. *Build. Environ.* **2003**, *38*, 147–159. [CrossRef]

6. Barnoos, V.; Oudbashi, O.; Shekofteh, A. The deterioration process of limestone in the Anahita Temple of Kangavar (West Iran). *Herit. Sci.* **2020**, *8*, 1–19. [CrossRef]

7. Janvier-Badosa, S.; Beck, K.; Brunetaud, X.; Al-Mukhtar, M. The occurrence of gypsum in the scaling of stones at the Castle of Chambord (France). *Environ. Earth Sci.* **2014**, *71*, 4751–4759. [CrossRef]

8. Rosado, T.; Silva, M.; Galvão, A.; Mirão, J.; Candeias, A.; Caldeira, A.T. A first insight on the biodegradation of limestone: The case of the World Heritage Convent of Christ. *Appl. Phys. A* **2016**, *122*, 1012. [CrossRef]

9. Bruno, N.; Roncella, R. HBIM for Conservation: A New Proposal for Information Modeling. *Remote Sens.* **2019**, *11*, 1751. [CrossRef]

10. Logothetis, S.; Stylianidis, E. BIM Open Source Software (OSS) for the documentation of cultural heritage. *Virtual Archaeol. Rev.* **2016**, *7*, 28–35. [CrossRef]

11. Doré, C.; Murphy, M. Integration of Historic Building Information Modeling (HBIM) and 3D GIS for recording and managing cultural heritage sites. In Proceedings of the 18th International Conference on Virtual Systems and Multimedia, Xi'an, China, 18–20 October 2012; pp. 369–376.

12. López, F.J.; Lerones, P.M.; Llamas, J.; Gómez-García-Bermejo, J.; Zalama, E. A Review of Heritage Building Information Modeling (H-BIM). *Multimodal Technol. Interact.* **2018**, *2*, 21. [CrossRef]

13. Del Giudice, M.; Osello, A. BIM for Cultural Heritage. *Int. Arch. Photogramm. Remote Sens. Spat. Inf. Sci.* **2013**, *5*, 225–229. [CrossRef]

14. Reinoso, J.F.; Rodríguez-Moreno, C.; Gómez-Blanco, A.J.; León-Robles, C.A. Cultural Heritage Conservation and Sustainability Based on Surveying and Modeling: The Case of the 14th Century Building Corral del Carbón (Granada, Spain). *Sustainability* **2018**, *10*, 1370. [CrossRef]

15. Themistocleous, K.; Agapiou, A.; Hadjimitsis, D. 3D Documentation and BIM Modeling of Cultural Heritage Structures Using UAVS: The Case of the Foinikaria Church. *Int. Arch. Photogramm. Remote Sens. Spat. Inf. Sci.* **2016**, *42*, 45–49. [CrossRef]

16. Oreni, D.; Brumana, R.; Della Torre, S.; Banfi, F.; Barazzetti, L.; Previtali, M. Survey turned into HBIM: The restoration and the work involved concerning the Basilica di Collemaggio after the earthquake (L'Aquila). *ISPRS Ann. Photogramm. Remote Sens. Spat. Inf. Sci.* **2014**, *2*, 267–273. [CrossRef]

17. Mercuri, F.; Cicero, C.; Orazi, N.; Paoloni, S.; Marinelli, M.; Zammit, U. Infrared Thermography Applied to the Study of Cultural Heritage. *Int. J. Thermophys.* **2015**, *36*, 1189–1194. [CrossRef]

18. Hällström, J.; Barup, K.; Grönlund, R.; Johansson, A.; Svanberg, S.; Palombi, L.; Lognoli, D.; Raimondi, V.; Cecchi, G.; Conti, C. Documentation of soiled and biodeteriorated facades: A case study on the Coliseum, Rome, using hyperspectral imaging fluorescence lidars. *J. Cult. Herit.* **2009**, *10*, 106–115. [CrossRef]

19. Yastikli, N. Documentation of cultural heritage using digital photogrammetry and laser scanning. *J. Cult. Herit.* **2007**, *8*, 423–427. [CrossRef]

20. Guarnieri, A.; Remondino, F.; Vettore, A. Digital photogrammetry and TLS data fusion applied to Cultural Heritage 3D modeling. *Int. Arch. Photogramm. Remote Sens. Spat. Inf. Sci.* **2006**, *36*, 1–6.

21. Del Pozo, S.; Herrero-Pascual, J.; Felipe-García, B.; Hernandez-Lopez, D.; Rodriguez-Gonzalvez, P.; González-Aguilera, D. Multispectral Radiometric Analysis of Façades to Detect Pathologies from Active and Passive Remote Sensing. *Remote Sens.* **2016**, *8*, 80. [CrossRef]

22. Pesci, A.; Bonali, E.; Galli, C.; Boschi, E. Laser scanning and digital imaging for the investigation of an ancient building: Palazzo d'Accursio study case (Bologna, Italy). *J. Cult. Herit.* **2012**, *13*, 215–220. [CrossRef]

23. Russo, M.; Carnevali, L.; Russo, V.; Savastano, D.; Taddia, Y. Modeling and deterioration mapping of façades in historical urban context by close-range ultra-lightweight UAVs photogrammetry. *Int. J. Arch. Herit.* **2019**, *13*, 549–568. [CrossRef]

24. Stepinac, M.; Gašparović, M. A Review of Emerging Technologies for an Assessment of Safety and Seismic Vulnerability and Damage Detection of Existing Masonry Structures. *Appl. Sci.* **2020**, *10*, 5060. [CrossRef]

25. Goodman, D.; Piro, S. *GPR Remote Sensing in Archaeology, Geotechnologies and the Environment*; Springer: Berlin/Heidelberg, Germany, 2013; Volume 9, ISBN 978-3-642-31857-3.

26. Fontul, S.; Solla, M.; Cruz, H.; Machado, J.S.; Pajewski, L. Ground Penetrating Radar Investigations in the Noble Hall of São Carlos Theater in Lisbon, Portugal. *Surv. Geophys.* **2018**, *39*, 1125–1147. [CrossRef]

27. Ferrara, C.; Barone, P.M. Detecting Moisture Damage in Archaeology and Cultural Heritage Sites Using the GPR Technique: A Brief Introduction. *Int. J. Archaeol.* **2015**, *3*, 57. [CrossRef]

28. Moropoulou, A.; Labropoulos, K.C.; Delegou, E.T.; Karoglou, M.; Bakolas, A. Non-destructive techniques as a tool for the protection of built cultural heritage. *Constr. Build. Mater.* **2013**, *48*, 1222–1239. [CrossRef]

29. Pérez-Gracia, V.; Caselles, J.; Clapés, J.; Martinez, G.; Osorio, R. Non-destructive analysis in cultural heritage buildings: Evaluating the Mallorca cathedral supporting structures. *NDT E Int.* **2013**, *59*, 40–47. [CrossRef]

30. Masini, N.; Persico, R.; Rizzo, E. Some examples of GPR prospecting for monitoring of the monumental heritage. *J. Geophys. Eng.* **2010**, *7*, 190–199. [CrossRef]

31. Pérez-Gracia, V.; García, F.; Pujades, L.G.; González-Drigo, R.; Di Capua, D. GPR survey to study the restoration of a Roman monument. *J. Cult. Herit.* **2008**, *9*, 89–96. [CrossRef]

32. Cataldo, R.; De Donno, A.; De Nunzio, G.; Leucci, G.; Nuzzo, L.; Siviero, S. Integrated methods for analysis of deterioration of cultural heritage: The Crypt of "Cattedrale di Otranto.". *J. Cult. Herit.* **2005**, *6*, 29–38. [CrossRef]

33. Garrido, I.; Solla, M.; Lagüela, S.; Fernández, N. IRT and GPR Techniques for Moisture Detection and Characterisation in Buildings. *Remote Sens.* **2020**, *20*, 6421. [CrossRef]

34. Solla, M.; Lagüela, S.; Fernández, N.; Garrido, I. Assessing Rebar Corrosion through the Combination of Nondestructive GPR and IRT Methodologies. *Remote Sens.* **2019**, *11*, 1705. [CrossRef]

35. Matera, L.; Persico, R.; Geraldi, E.; Sileo, M.; Piro, S. GPR and IRT tests in two historical buildings in Gravina in Puglia. *Geosci. Instrum. Methods* **2016**, *5*, 541–550. [CrossRef]

36. Solla, M.; Asorey-Cacheda, R.; Núñez-Nieto, X.; Conde, B. Evaluation of historical bridges through recreation of GPR models with the FDTD algorithm. *NDT E Int.* **2016**, *77*, 19–27. [CrossRef]

37. Sfarra, S.; Bendada, A.; Ibarra-Castanedo, C.; Ambrosini, D.; Paoletti, D.; Maldague, X. Santa Maria di Collemaggio Church (L'Aquila, Italy): Historical Reconstruction by Non-Destructive Testing Techniques. *Int. J. Arch. Herit.* **2015**, *9*, 367–390. [CrossRef]

38. Carlomagno, G.M.; Di Maio, R.; Fedi, M.; Meola, C. Integration of infrared thermography and high-frequency electromagnetic methods in archaeological surveys. *J. Geophys. Eng.* **2011**, *8*, S93–S105. [CrossRef]

39. Rizo-Maestre, C.; González-Avilés, Á.; Galiano-Garrigós, A.; Andújar-Montoya, M.D.; Puchol-García, J.A. UAV BIM: Incorporation of Photogrammetric Techniques in Architectural Projects with Building Information Modeling Versus Classical Work Processes. *Remote Sens.* **2020**, *12*, 2329. [CrossRef]

40. Mahmood, B.; Han, S.; Lee, D. BIM-based Registration and Localization of 3D Point Clouds of Indoor Scenes Using Geometric Features for Augmented Reality. *Remote Sens.* **2020**, *12*, 2302. [CrossRef]

41. Bassier, M.; Vergauwen, M.; Poux, F. Point Cloud vs. Mesh Features for Building Interior Classification. *Remote Sens.* **2020**, *12*, 2224. [CrossRef]

42. Bassier, M.; Vergauwen, M. Topology Reconstruction of BIM Wall Objects from Point Cloud Data. *Remote Sens.* **2020**, *12*, 1800. [CrossRef]

43. Kim, S.; Kim, S.; Lee, D. 3D Point Cloud and BIM-Based Reconstruction for Evaluation of Project by As-Planned and As-Built. *Remote Sens.* **2020**, *12*, 1457. [CrossRef]

44. Andriasyan, M.; Moyano, J.; Nieto-Julián, J.E.; Antón, D. From Point Cloud Data to Building Information Modelling: An Automatic Parametric Workflow for Heritage. *Remote Sens.* **2020**, *12*, 1094. [CrossRef]

45. Pierdicca, R.; Paolanti, M.; Matrone, F.; Martini, M.; Morbidoni, C.; Malinverni, E.S.; Frontoni, E.; Lingua, A.M. Point Cloud Semantic Segmentation Using a Deep Learning Framework for Cultural Heritage. *Remote Sens.* **2020**, *12*, 1005. [CrossRef]

46. Tran, H.; Khoshelham, K. Procedural Reconstruction of 3D Indoor Models from Lidar Data Using Reversible Jump Markov Chain Monte Carlo. *Remote Sens.* **2020**, *12*, 838. [CrossRef]

47. Frías, E.; Díaz-Vilariño, L.; Balado, J.; Lorenzo, H. From BIM to Scan Planning and Optimization for Construction Control. *Remote Sens.* **2019**, *11*, 1963. [CrossRef]

48. Bassier, M.; Vergauwen, M. Clustering of Wall Geometry from Unstructured Point Clouds Using Conditional Random Fields. *Remote Sens.* **2019**, *11*, 1586. [CrossRef]

49. Tsilimantou, E.; Delegou, E.T.; Nikitakos, I.A.; Ioannidis, C.; Moropoulou, A. GIS and BIM as Integrated Digital Environments for Modeling and Monitoring of Historic Buildings. *Appl. Sci.* **2020**, *10*, 1078. [CrossRef]

50. Alhaidary, H.; Al-Tamimi, A.K.; Al-Wakil, H. The combined use of BIM, IR thermography and HFS for energy modelling of existing buildings and minimising heat gain through the building envelope: A case-study from a UAE building. *Adv. Build. Energy Res.* **2019**, 1–24. [CrossRef]

51. Coli, M.; Ciuffreda, A.L.; Micheloni, M. An Informative Content 3d Model for the Hall Holding the Resurrection of Christ by Piero Della Francesca Mural Painting at Sansepolcro, Italy. *Int. Arch. Photogramm. Remote Sens. Spat. Inf. Sci.* **2019**, *2*, 435–442. [CrossRef]

52. Bruno, S.; Fatiguso, F. Building conditions assessment of built heritage in historic building information modeling. *Int. J. Sustain. Dev. Plan.* **2018**, *13*, 36–48. [CrossRef]

53. Shrestha, S.; Reina Ortiz, M.; Gutland, M.; Morris, M.; Napolitano, R.; Santana-Quintero, M.; Erochko, J.; Kawan, S. Digital Recording and Non Destructive Investigation of Nyatapola Temple after Gorkha Earthquake 2015. In Proceedings of the 19th ICOMOS General Assembly & Scientific Symposium 2017, New Delhi, India, 11–15 December 2017.

54. Barazzetti, L.; Banfi, F.; Brumana, R.; Previtali, M.; Roncoroni, F. BIM from Laser Scans . . . Not Just for Buildings: Nurbs-Based Parametric Modeling of a Medieval Bridge. *ISPRS Ann. Photogramm. Remote Sens. Spat. Inf. Sci.* **2016**, 51–56. [CrossRef]

55. Lagüela, S.; Díaz-Vilariño, L.; Armesto, J.; Arias, P. Non-destructive approach for the generation and thermal characterization of an as-built BIM. *Constr. Build. Mater.* **2014**, *51*, 55–61. [CrossRef]

56. Gomes, S.A. The Monastery of Our Lady of Victory in the 15th Century (in Portuguese: *O Mosteiro de Santa Maria da Vitória no Século XV*). Master's Thesis, Faculty of Humanities of University of Coimbra, Institute of Art History, Coimbra, Portugal, 1990.

57. Soares, C. *The Restoration of Monastery of Batalha: Historic Quarries, Building Site and Master Masons (in Portuguese: O Restauro do Mosteiro da Batalha: Pedreiras Históricas, Estaleiro de Obras e Mestres Canteiros)*; Magno Edições: Leiria, Portugal, 2001.

58. Aires-Barros, L.A.; Baptista Neto, M.J.; Soares, C. The Monastery of Batalha (Portugal): Restoration Works and Historic Quarries, a Preliminary Study. In *IV Congreso Internacional de Rehabilitación del Patrimonio Arquitectónico y Edificación*; CICOP: La Habana, Cuba, 1998; pp. 384–386.

59. Trimble. *eCognition Developer: User Guide*; Trimble: Munich, Germany, 2019.

60. Sandmeier, K.J. ReflexW Manual. Available online: https://www.sandmeier-geo.de (accessed on 30 July 2020).

61. Solla, M.; González-Jorge, H.; Álvarez, M.X.; Arias, P. Application of non-destructive geomatic techniques and FDTD modeling to metrical analysis of stone blocks in a masonry wall. *Constr. Build. Mater.* **2012**, *36*, 14–19. [CrossRef]

62. Lagüela, S.; Solla, M.; Puente, I.; Prego, F.J. Joint use of GPR, IRT and TLS techniques for the integral damage detection in paving. *Constr. Build. Mater.* **2018**, *174*, 749–760. [CrossRef]

63. Avdelidis, N.; Moropoulou, A. Applications of infrared thermography for the investigation of historic structures. *J. Cult. Herit.* **2004**, *5*, 119–127. [CrossRef]

64. Khoshelham, K.; Díaz-Vilariño, L. 3D Modelling of Interior Spaces: Learning the Language of Indoor Architecture. *Int. Arch. Photogramm. Remote Sens. Spat. Inf. Sci.* **2014**, 321–326. [CrossRef]

65. Puente, I.; Solla, M.; González-Jorge, H.; Arias, P. NDT Documentation and Evaluation of the Roman Bridge of Lugo Using GPR and Mobile and Static LiDAR. *J. Perform. Constr. Facil.* **2015**, *29*. [CrossRef]

66. Shen, Y.; Wang, J.; Puente, I. A Novel Baseline-Based Method to Detect Local Structural Changes in Masonry Walls Using Dense Terrestrial Laser Scanning Point Clouds. *IEEE Sens. J.* **2020**, *20*, 6504–6515. [CrossRef]

67. Puente, I.; Lindenbergh, R.; Van Natijne, A.; Esposito, R.; Schipper, R. Monitoring of Progressive Damage in Buildings Using Laser Scan Data. *Int. Arch. Photogramm. Remote Sens. Spat. Inf. Sci.* **2018**, *42*, 923–929. [CrossRef]

68. Laser Scanner Faro Focus 3D X330—User's Manual. Faro Technologies, Inc. Available online: http://www2.faro.com/ (accessed on 24 July 2020).

69. Gomes, S.A. *Parochial News and Memories of the Eighteenth Century–3: Batalha (in Portuguese: Notícias e Memórias Paroquiais Setecentistas–3: Batalha)*; Palimage and Centro de História da Sociedade e da Cultura: Coimbra, Portugal, 2005; Volume 3.